Particle Accelerators, 1992, Vols. 37–38, pp. 181–189
Reprints available directly from the publisher
Photocopying permitted by license only

THEORETICAL STUDY OF THE LONGITUDINAL INSTABILITY AND PROPOSED EXPERIMENT†

J. G. WANG, M. REISER, W. M. GUO and D. X. WANG

Laboratory for Plasma Research and Department of Electrical Engineering, University of Maryland, College Park, Maryland 20742.

(Received 3 January 1991)

A theoretical model for the longitudinal instability in a transport pipe with general wall impedance is presented. The results show that a capacitive wall tends to stabilize the beam. Design features for an experimental study of the instability with an electron beam in a pure resistive-wall environment will be discussed, including the design parameters, setup and components for the experiment.

1 INTRODUCTION

The induction linac is being studied in the USA as a driver for Heavy Ion Inertial Fusion. When the heavy ions are accelerated by the induction gaps, the beam sees a gap impedance along the accelerator and transport channels. Theoretical studies predict that there is a resistive-wall instability which is detrimental to the beam.

The analysis of the instability in this paper takes into account the general wall impedance of the transport pipe. It predicts that the instability could be reduced by a capacitive wall and enhanced by an inductive wall. It also shows that the temporal growth rate of the resistive-wall instability is inversely proportional to the square root of the mass of the particles. An experiment to study the instability with heavy ions would be costly because of the large mass of the ions which requires a long distance to observe the effect.

We plan to study experimentally the longitudinal instability with electrons. Specifically, an electron gun has been designed and constructed to produce a beam of 5 to 50 ns in width, 2.5 keV in energy, and a maximum of 160 mA in current. An induction linac following the gun will impart a small head-to-tail energy spread to the beam to balance beam expansion in the longitudinal direction. The beam is further matched to a resistive-wall channel of a few meters in length with uniform solenoidal magnetic field. Various diagnostics will be used to determine the instability in this transport experiment. Comparison with simulation could provide useful information for heavy ion induction linacs.

† Research supported by the U.S. Department of Energy.

2 BEAM LONGITUDINAL INSTABILITY WITH GENERAL WALL IMPEDANCE

The longitudinal beam dynamics can be described by the linearized cold one-dimensional fluid model, which consists of the continuity equation and momentum transfer equation[1,2,3]:

$$\begin{cases} \dfrac{\partial \lambda_1}{\partial t} + v_0 \dfrac{\partial \lambda_1}{\partial z} + \lambda_0 \dfrac{\partial v_1}{\partial z} = 0 \\ \dfrac{\partial v_1}{\partial t} + v_0 \dfrac{\partial v_1}{\partial z} \approx \eta E_z \end{cases}, \tag{1}$$

where λ and v are the line charge density and the particle velocity, the subscripts 0 and 1 representing the unperturbed and perturbed quantities, respectively, E_z is the induced longitudinal electrical field by the a.c. component of the beam current, and $\eta = e/m$ denotes the ratio of the charge and mass of the charged particles. For a nonrelativistic beam under the long wavelength condition, the field E_z can be calculated as[4]

$$E_z = -\frac{g}{4\pi\varepsilon_0} \frac{\partial \lambda_1}{\partial z} + E_w, \tag{2}$$

where E_w is the field on the pipe wall of the transport channel, ε_0 is the permittivity of free space, and g is a geometric factor given by

$$g = 2 \ln \frac{b}{a} + \frac{2}{3}, \tag{3}$$

with a and b as the beam radius and pipe radius, respectively. In the derivation of Eq. (3), a uniform beam profile is assumed and the average beam self-field over the whole beam cross section is taken into account.

In general, the pipe wall has an impedance per unit length, given in the frequency domain by

$$Z_w = R(\omega) + iX(\omega), \tag{4}$$

where $R(\omega)$ and $X(\omega)$ are the real and imaginary parts of the complex impedance. The field E_w is generated by the perturbed beam image current on the wall and can be expressed by

$$E_w = -\lambda_1 v^* R(\omega_0) + v^{*2} \frac{X(\omega_0)}{\omega_0} \frac{\partial \lambda_1}{\partial z}, \tag{5}$$

where $\omega_0 = kv_0$ is the characteristic frequency of the instability. The velocity v^* with which the perturbation propagates should be very close to the mean speed of particles and is approximated as v_0 in the following analysis. It is not difficult to verify the validity of Eq. (5) with simple circuit models, while a derivation of this formula is left in a forthcoming paper. Therefore, the total longitudinal field (2) acting

on the beam is

$$E_z \approx -\left(\frac{g}{4\pi\varepsilon_0} - v_0^2 \frac{X(\omega_0)}{\omega_0}\right) \frac{\partial \lambda_1}{\partial z} - \lambda_1 v_0 R(\omega_0). \tag{6}$$

Equation (1) along with Eq. (6) can be solved by using a Laplace transform in time and a Fourier transform in space; that leads to the dispersion relation

$$D(s, k) = (s + ikv_0)^2 + k^2\eta\left(\frac{g}{4\pi\varepsilon_0} - v_0^2 \frac{X(\omega_0)}{\omega_0}\right)\lambda_0 - ik\eta\lambda_0 v_0 R(\omega_0). \tag{7}$$

In the parameter range of interest, the dispersion equation $D(s, k) = 0$ may be solved approximately to give rise to the perturbed wave frequency and the temporal growth rate

$$\begin{cases} \omega_r \approx kv_0 \pm k\left[\eta\lambda_0\left(\dfrac{g}{4\pi\varepsilon_0} - v_0^2 \dfrac{X(\omega_0)}{\omega_0}\right)\right]^{1/2} \\ \omega_i \approx \mp \dfrac{1}{2} v_0 R(\omega_0)\left(\dfrac{\eta\lambda_0}{\dfrac{g}{4\pi\varepsilon_0} - v_0^2 \dfrac{X(\omega_0)}{\omega_0}}\right)^{1/2}. \end{cases} \tag{8}$$

This equation is correct only when k is real as implicitly defined by the Fourier transform in space. Equation (8) shows that the slow wave grows at the expense of the beam energy. For a pure resistive wall, in the low-frequency approximation where $R(\omega_0) = R$ and $X(\omega_0) = 0$, the slow-wave growth rate is

$$\omega_i \approx \frac{1}{2} v_0 R\left(\frac{\eta\lambda_0 4\pi\varepsilon_0}{g}\right)^{1/2}. \tag{9}$$

If the pipe wall is inductive, e.g., $Z = R + i\omega_0 L$, one gets

$$\omega_i \approx \frac{1}{2} v_0 R\left(\frac{\eta\lambda_0}{\dfrac{g}{4\pi\varepsilon_0} - Lv_0^2}\right)^{1/2}. \tag{10}$$

Thus, the addition of an inductive component increases the growth rate in comparison with Eq. (9). For a capacitive wall modeled by a circuit of R and C in parallel, Eq. (8) can be rewritten as

$$\omega_i \approx \frac{1}{2} v_0 \frac{R}{1 + \omega_0^2 R^2 C^2}\left(\frac{\eta\lambda_0}{\dfrac{g}{4\pi\varepsilon_0} + \dfrac{v_0^2 R^2 C}{1 + \omega_0^2 R^2 C^2}}\right)^{1/2}. \tag{11}$$

As expected, the growth rate of the slow wave is reduced when a capacitance is added. This result agrees with Reference 1, which states that, in general, the capacity reduces growth rates, compared with the case of pure resistance by lowering the impedance as frequency increases. Reference 5 analyses the resistive instability growth rates in

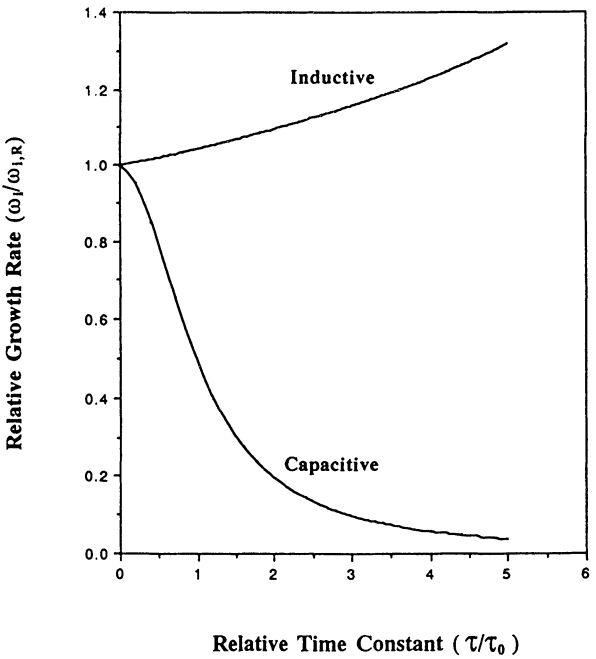

FIGURE 1 Relative growth rate $\omega_i/\omega_{i,R}$ vs. the relative time constant τ/τ_0 where ω_i is the growth rate from Eqs. (9)–(11); $\omega_{i,R}$ is specified as the growth rate for a pure resistive wall; $\tau = RC$ for the capacitive wall, or $\tau = L/R$ for the inductive wall; and $\tau_0 = 1/\omega_0$. It is assumed that $v_0 = 0.1c$, $R = 100\ \Omega/\text{m}$, and $\omega_0 = 2\pi \times 10^7\ \text{s}^{-1}$ in this example.

the modules represented by a parallel R, L, C circuit. Its results can also be recovered from Eq. (7).

To illustrate the results from Eqs. (9)–(11), Figure 1 shows the relative growth rate versus the time constant of the wall impedance. In this example the growth rate for a pure resistive wall is set to unity. The beam is supposed to have a velocity of $\beta = 0.1$. The pipe wall resistance is $100\ \Omega/\text{m}$ and the characteristic frequency is assumed to be 10 MHz. The lower branch of the plot is for the capacitive wall with $\tau/\tau_0 = RC\omega_0$ while the upper branch is for the inductive wall with $\tau/\tau_0 = \omega_0 L/R$. The growth rate for the capacitive wall decreases rapidly when the capacitance is increased. This dependence is not sensitive to the beam parameters. By contrast, the growth rate for an inductive wall is highly beam-velocity dependent.

3 DESIGN STUDY OF THE RESISTIVE-WALL INSTABILITY EXPERIMENT

Equation (8) shows that the temporal growth rate of the resistive-wall instability is inversely proportional to the square root of the mass of the beam particles. An

experiment to study the instability with heavy ions would be costly because of the large mass of the ions which requires a long distance to observe the effect. With electrons, the experiment could be done at a small scale and much less cost.

For a pure resistive wall, the phase velocity of the slow wave in the beam frame and the growth rate can be derived from Eq. (8) as

$$\begin{cases} v_{ph} \approx v_0 \left(\frac{1}{2} Kg\right)^{1/2} \\ \omega_i \approx \pi \varepsilon_0 v_0^2 R \left(\frac{2K}{g}\right)^{1/2}, \end{cases} \tag{12}$$

where K is the generalized perveance and, for non-relativistic electrons, is given by

$$K = 1.515 \times 10^4 \frac{I(A)}{V^{3/2}(V)}, \tag{13}$$

with I and V as the beam current and energy equivalent voltage, respectively. The e-fold instability growth length in the beam frame is determined by

$$l_g = \frac{g}{2\pi \varepsilon_0 v_0 R}. \tag{14}$$

For a beam pulse of the width T, the number of e-folds in the growth from the beam head to tail is

$$n = R v_0^2 \frac{2\pi \varepsilon_0}{g} T. \tag{15}$$

The number of e-folds per unit channel length is given by

$$N = \left(\frac{1}{2} \eta \pi^2 \varepsilon_0^2\right)^{1/4} \left(\frac{I}{g V^{1/2}}\right)^{1/2} R, \tag{16}$$

which is proportional to the wall resistance, and to the square root of the beam current, and is inversely proportional to the fourth root of the beam voltage. For a perturbation starting from the beam head at the channel entrance and ending at the beam tail at the channel exit, the relationship between the pulse length T and the channel length L is given by

$$T = \frac{L}{2} \left(\frac{Kg}{\eta V}\right)^{1/2}. \tag{17}$$

In order to observe the instability in a reasonable short distance, an electron beam has been designed with the following parameters: beam pulse width of 5 ns, beam voltage of 2.5 keV, and beam current of around 100 mA. This corresponds to about 15 cm of beam pulse length in space. Assuming a resistance of 10 kΩ/m and $g = 2$, Eqs. (14)–(16) yield $l_g \cong 12.2$ cm, $n \cong 1.2$ and $N \cong 0.91$. A transport channel of 1.3 meters in length would satisfy Eq. (17). These parameters will be scaled in the experiment.

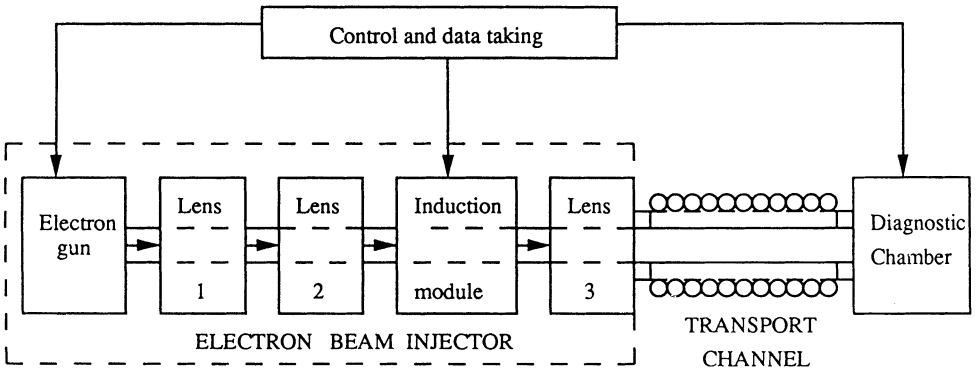

FIGURE 2 Schematic diagram of the resistive-wall instability experiment.

A schematic diagram of the experimental setup is shown in Figure 2. An electron beam injector, originally designed for longitudinal pulse compression experiments, is employed as the beam pulse source. The injector consists of a variable-perveance gridded electron gun, three matching lenses and an induction acceleration module. The electron gun produces a beam pulse with the desired parameters. The matching lenses confine the beam in the transverse direction. The induction acceleration module imparts a small head-to-tail energy spread to the beam to balance beam expansion in the longitudinal direction due to space charge. The beam from the injector is guided into a resistive-wall channel of a few meters in length with a uniform solenoidal magnetic field to provide transverse focusing. The end diagnostic chamber will pick up all the necessary information to determine the instability in this transport experiment. The components for the injector have been constructed and extensively tested. The assembling of the injector system is underway. The coating of the transport channel with resistive material is in progress. The various diagnostic equipments are to be built. The design and performance characteristics of the major components of the system are described briefly as follows:

3.1 Electron Gun

The detailed information about the gun design and performance characteristics can be found in Reference 6. This is a variable-perveance gridded gun with Pierce geometry electrodes. The gun perveance can vary from 0.22×10^{-6} to $1.35 \times 10^{-6}\ AV^{-3/2}$ by adjusting the A–K gap. The maximum beam energy from the gun is 10 keV and the beam current can be as high as 160 mA at an anode voltage of 2.5 kV. The beam current is controlled by a fast grid-cathode pulse which is adjustable in length from a few nanosecond up to hundreds of nanoseconds. A 5 ns grid-cathode pulse is shown in Figure 3, where one still can see a flat top of the pulse and a small risetime of less than 1 ns. The beam pulse shape should resemble the grid-cathode pulse waveform. The grid-cathode pulse can be modulated with a perturbation to initiate the beam instability.

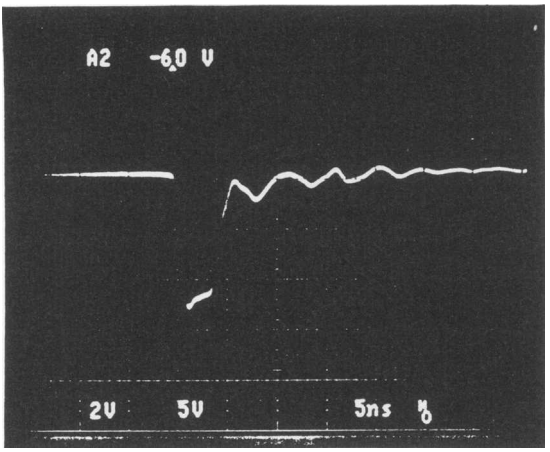

FIGURE 3 Example of the grid-cathode pulse, which shows 5 ns width and less 1 ns risetime.

3.2 *Induction Acceleration Module*

Reference 7 gives a detailed description of the performance analysis and testing results of this device. Originally designed for pulse compression experiments, the compact induction acceleration module produces a quadratic time-varying voltage on its gap during about 50 ns. The gap voltage as a function of time from the test is shown in Figure 4. This gap voltage waveform is determined by the modulator consisting of

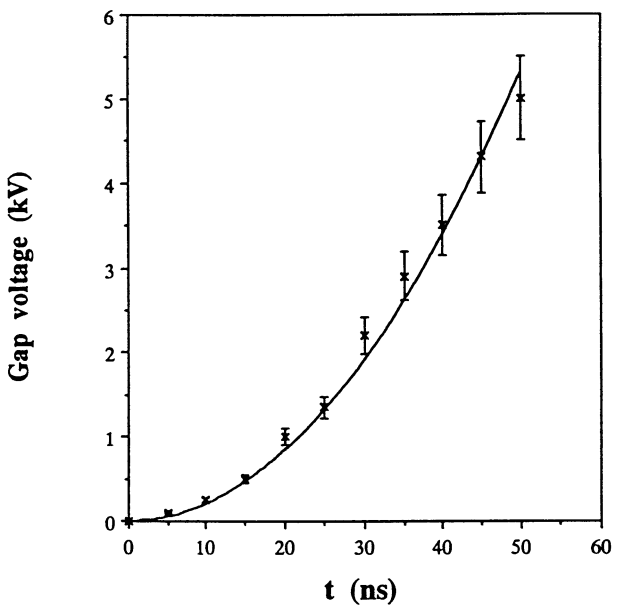

Figure 4 Induction gap voltage vs. time in the first 50 ns where the data points were from the measurement and the smooth curve was an ideal fitting to t^2 curve.

a few inductances and capacitances. It is easy to change this waveform as one desires. For the resistive-wall instability experiment with a beam pulse of 5 ns, the induction module will only impart a small energy difference from the beam head to tail to balance the longitudinal expansion. The induction module should be synchronized with the electron gun within 1 ns during operation.

3.3 Resistive-Wall Pipe

Production of a resistive-wall pipe follows the work of Reference 8. Specifically, a glass tube of 3.8 cm in diameter and a couple of meters in length in the first phase of the experiment will be coated with tin oxide. The design goal for the resistance is a few thousand ohms per meter. The tube is located inside and coaxial with a long solenoid which produces a uniform magnetic focusing field of around 100 gauss. This field provides forces in transverse direction to balance space charge forces. An identical pipe with good conductivity will also be employed for comparison study.

3.4 Diagnostics

The diagnostics in the experiment includes accurate measurement of the beam current waveform, beam profile, time-resolved beam energy, etc. An existing Faraday cup is to be improved to achieve fast response: less than 1 ns in risetime. A fast Rogoski coil will be used to make non-destructive beam current measurement at the input and output of the transport channel. A time-resolved spectrum analyzer is underway for design and construction.

4 SUMMARY

The cold one-dimensional fluid model has been used to analyze the longitudinal instability in a beam transport channel with general wall impedances. The temporal growth rate of the instability can be dramatically reduced by a capacitive component of wall impedance along the transport channel. By contrast, the inductive wall component would enhance the instability.

Based on the result of this analysis, an experiment to study the resistive-wall instability with an electron beam has been designed. An electron beam injector producing the desired beam parameters has been constructed and its components have been extensively tested. Manufacturing of a resistive wall and preparation of the diagnostic tools are underway. The experimental results will be reported elsewhere in the near future.

REFERENCES

1. E. P. Lee and L. Smith, in *Proceedings of the 1990 Linear Accelerator Conference* (Albuquerque, NM, 1990).
2. E. P. Lee, Proceedings of the 1981 Linear Accelerator Conference, Santa Fe, NM, October 19–23, 1981.
3. J. Bisognano, I. Haber, L. Smith, and A. Sternlieb, *IEEE Trans. Nucl. Sci.* **NS-28**, 3 (June 1981).
4. A. Hofmann, CERN report 77-13, p. 139 (CERN, Geneva, 1977).

5. L. Smith, Lawrence Berkeley Laboratory internal note HIFAR-Note-217 (1988).
6. J. G. Wang, E. Boggasch, P. Haldman, D. Kehne, M. Reiser, T. Shea, and D. X. Wang, IEEE Trans. Electron Devices **37** (12) (December 1990), pp. 2622–2628.
7. J. G. Wang, D. X. Wang, E. Boggasch, D. Kehne, M. Reiser, and T. Shea, *Nucl. Instrum. Meth. A* **301**, (1991) pp. 19–26.
8. C. K. Birdsall, G. R. Brewer, and A. V. Haeff, Proc. I.R.E. **41**, 7 (July 1953).